Stress Corrosion Cracking Behavior of Wrought Magnesium Alloy AZ31 and AZ61 under Controlled Cathodic Potentials

Toshifumi Kakiuchi[1,*], Yoshihiko Uematsu[1]
Masaki Nakajima[2], Yuki Nakamura[2], Kosuke Miyagi[3]

[1] Department of Mechanical and Systems Engineering, Gifu University, Gifu, 501-1193, Japan
[2] Department of Mechanical Engineering, Toyota National College of Technology, Toyota, 471-8525, Japan
[3] Howa Machinery Ltd., Kiyosu, 462-8601, Japan
* Corresponding author: kakiuchi@gifu-u.ac.jp

Abstract The stress corrosion cracking (SCC) tests were performed using the wrought magnesium alloys, AZ31, AZ61 and T5 heat treated AZ61 (AZ61-T5) in a NaCl solution under the controlled cathodic potential in order to investigate the effects of the anodic dissolution and the hydrogen embrittlement on the SCC behavior. The crack growth rate (da/dt) of AZ31 was faster than those of AZ61 and AZ61-T5 under the same cathodic potential. The threshold stress intensity factor for SCC propagation (K_{ISCC}) of AZ31 was lower than those of AZ61 and AZ61-T5, and K_{ISCC} of AZ61-T5 was lower than that of AZ61, which is attributed to the difference of resistance to anodic dissolution. In AZ31 and AZ61, K_{ISCC} under the cathodic potential of -2.5 V was higher than those under the other cathodic potentials. In all materials, K_{ISCC} under the cathodic potential of -1.4 V was lower than those under the cathodic potentials of -3.0 V and -4.0 V. By the observations on the fracture surfaces after the SCC tests, less corrosion products were observed on the fracture surfaces under the cathodic potentials of -3.0 V and -4.0 V than on the fracture surfaces under the cathodic potential of -1.4 V.

Keywords Stress corrosion cracking, Magnesium alloy, Hydrogen embrittlement, Anodic dissolution

1. Introduction

In the recent years, light materials have been promoted to be applied in a wide variety of applications, especially in structural components of transportation machines such as airplanes and ground vehicles to reduce fuel consumption. Magnesium (Mg) alloys are the lightest among all available metals in practical use and have high specific strengths. So Mg alloys are expected as structural materials for transportation machines. However Mg alloys are sensitive to corrosion and exhibit the poor corrosion resistance compared with the other light metals such as aluminum and titanium alloys. Thus it is important to understand the corrosion properties of Mg alloys. Especially, the stress corrosion cracking (SCC) behavior is important since it could cause sudden and fatal failures.

The SCC could be attributed to the combined effects of the anodic dissolution and the hydrogen embrittlement. Especially the hydrogen embrittlement plays an important role in the SCC of Mg alloys. Previously the present authors have performed the SCC tests using the wrought Mg alloy AZ31 in a NaCl solution under the controlled cathodic potential to decouple the effects of anodic dissolution and hydrogen embrittlement and have investigated the SCC behavior [1]. In the present study, the similar SCC tests were performed using the wrought Mg alloys AZ31, AZ61 and T5 heat treated AZ61 to investigate the effects of the anodic dissolution and the hydrogen embrittlement on the SCC behavior of Mg alloys.

2. Experimental details

2.1. Material and specimen

The materials used were the wrought Mg alloys AZ31 and AZ61. The chemical compositions and

the mechanical properties of the materials are shown in Table 1 and Table 2, respectively. The β phase of Mg alloy, i.e., $Mg_{17}Al_{12}$, is more sensitive to hydrogen embrittlement than the matrix. Hence it is expected that the SCC behavior is dependent on the content of β phase. To investigate the effect of β phase on the SCC behavior, the T5 heat treated AZ61 (AZ61-T5) in which β phases were precipitated along the grain boundaries was also used. The T5 heat treatment was set to hold the material at the temperature of 170 ºC for 42 hours followed by cooling in the air. Fig. 1 shows the optical micrographs showing the microstructures of (a) AZ31, (b) AZ61 and (c) AZ61-T5. Fig. 2 shows the micrograph by a scanning electron microscope (SEM) showing the microstructure of AZ61-T5 in the high resolution. The β phase precipitates were observed along the grain boundaries.

Table 1. Chemical compositions of materials (wt%)

Material	Al	Zn	Mn	Si	Cu	Ni	Fe	Mg
AZ31	2.7	0.79	0.44	0.004	0.0011	0.0009	0.0012	Bal.
AZ61	5.8	0.65	0.29	0.01	0.002	0.002	0.002	Bal.

Table 2. Mechanical properties of materials

Material	0.2% proof stress, $\sigma_{0.2}$ (MPa)	Tensile strength, σ_B (MPa)	Elongation, δ (%)	Vickers hardness, *HV*	Elastic modulus, *E* (GPa)
AZ31	170	248	17	54	46
AZ61	192	301	19	62	44

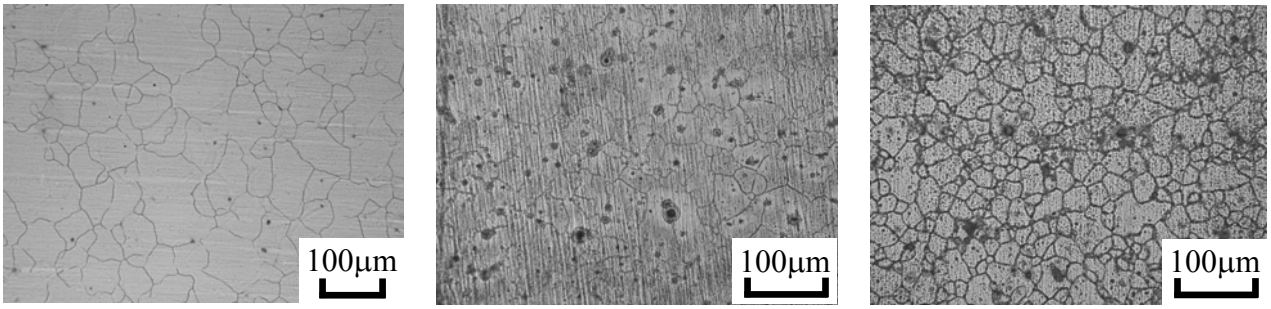

(a) AZ31 (b) AZ61 (c)AZ61-T5

Figure 1. Microstructures of materials

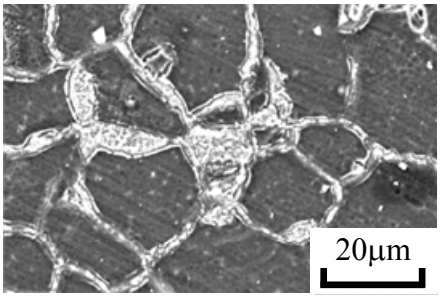

Figure 2. SEM micrograph showing β phase precipitates along grain boundaries in AZ61-T5

For the SCC tests, compact tension (CT) specimens with the configuration of a width of 50.8 mm and a thickness of 6 mm were fabricated by machining from the materials. Fig. 3 shows the configuration of a CT specimen. Prior to the SCC tests, a pre-crack with a length of 2 mm was introduced from the artificial notch root of CT specimen. Pre-cracks were introduced by a fatigue test at the frequency of 10Hz, the stress ratio of 0.1 and the initial stress intensity factor range ΔK_I of 3 MPa $m^{1/2}$.

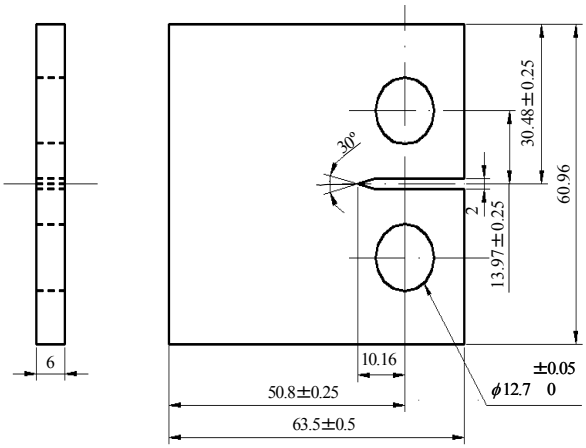

Figure 3. CT specimen configuration

2.2. Stress corrosion cracking test

Fig. 4 shows the schematic illustration of SCC test apparatus. The crack length was monitored by a crack gauge bonded to a crack-expected part of CT specimen. In the SCC tests of AZ61 and AZ61-T5, crack gauges were peeled off frequently since the crack growth rate was low and the testing time was long. So a traveling microscope was also used to monitor the crack length of AZ61 and AZ61-T5 specimens. A CT specimen with a fatigue pre-crack was attached to the creep testing machine equipped with a 3% NaCl solution tank. Prior to the loading, SCC test specimens were held in a NaCl solution at a given cathodic potential for 24 hours under no-loaded condition to charge hydrogen. After the loading, the load was gradually increased every 24 hours until a crack initiated to propagate. Once a crack initiated to propagate, the load was sustained and the crack growth was monitored by a crack gauge or a traveling microscope. In the solution tank, the Ag/AgCl and Pt electrodes were set for the reference and counter electrodes, respectively and the cathodic potential of specimen was controlled by means of a potentiostat (HA-303: HOKUTO DENKO Corp.). The cathodic potentials were controlled to be -1.4 V, -2.5 V, and -3.0 V for AZ31; 0 V, -1.4 V, -2.5 V and -4.0 V for AZ61; and -1.4 V and -4.0 V for AZ61-T5.

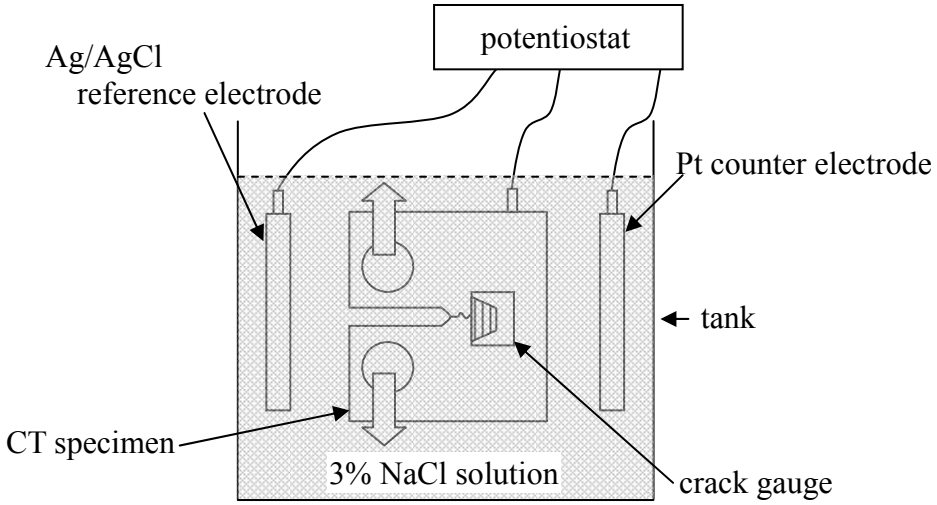

Figure 4. SCC test apparatus

The Pourbaix diagram of Mg [2], which shows the stable phase of an electrochemical system, is shown in Fig. 5. The pH of 3% NaCl solution is 7. The test conditions are also plotted in Fig. 5. It is

considered that the SCC behavior is dominated by the anodic dissolution in the corrosion region and by the hydrogen embrittlement in the immunity region. According to the Pourbaix diagram, the cathodic potential of -1.4 V corresponds to the corrosion region under which the SCC behavior is dominated by the anodic dissolution. The cathodic potentials of -3.0 V and -4.0 V correspond to the immunity region under which the SCC behavior is dominated by the hydrogen embrittlement. The cathodic potential of -2.5 V corresponds to the boundary between the corrosion and immunity regions. The SCC test conditions of cathodic potentials and electrochemical phases for each material are summarized in Table 3.

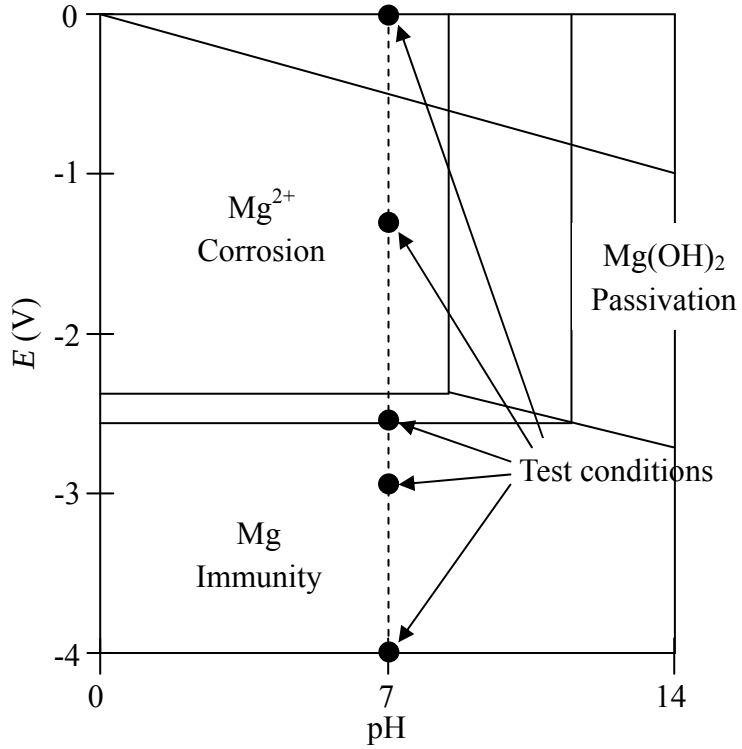

Figure 5. Pourbaix diagram for magnesium

Table 3. SCC test condition

Material	Cathodic potential				
	Corrosion region of Mg			Immunity region of Mg	
	0V	-1.4V	-2.5V	-3.0V	-4.0V
AZ31		Tested	Tested	Tested	
AZ61	Tested	Tested	Tested		Tested
AZ61-T5		Tested			Tested

3. Experimental results

3.1. Crack growth behavior

Fig. 6 shows the relationship between the crack length, *a*, and the testing time, *t*, after the crack initiated to propagate in a stable manner. The SCC behavior depends on the material, i.e., AZ31 specimens fractured more rapidly than AZ61 and AZ61-T5 specimens, and AZ61-T5 specimens fractured more rapidly than AZ61 specimens. In all materials, the final crack lengths were shorter and specimens fractured more rapidly under the cathodic potentials of -3.0 V and -4.0 V which correspond to the immunity region than under the cathodic potentials of 0 V and -1.4 V which

correspond to the corrosion region, except for the AZ61 specimen under the cathodic potential of -1.4 V. Fig. 7 shows the relationship between the crack growth rate, da/dt, and the stress intensity factor, K_I. Crack growth rates of AZ31 are much faster than those of AZ61 and AZ61-T5, and those of AZ61-T5 are faster than those of AZ61 under the same cathodic potentials. The crack growth rate of AZ31 is not sensitive to the change of K_I values especially under the cathodic potential of -3.0 V. The relationship between the threshold stress intensity factor for the SCC propagation, K_{ISCC}, and the cathodic potential, E, is summarized and shown in Fig. 8. In AZ31, K_{ISCC} under the cathodic potential of -2.5 V is higher than those under the cathodic potentials of -1.4 V and -3.0 V. This tendency is the same in AZ61, i.e., K_{ISCC} of AZ61 under the cathodic potential of -2.5 V is higher than those under the other cathodic potentials. In AZ61, K_{ISCC} under the cathodic potential of 0 V is the same as that under the cathodic potential of -1.4 V. In all materials, K_{ISCC} under the cathodic potential of -1.4 V is lower than that under the cathodic potentials of -3.0 V and -4.0 V.

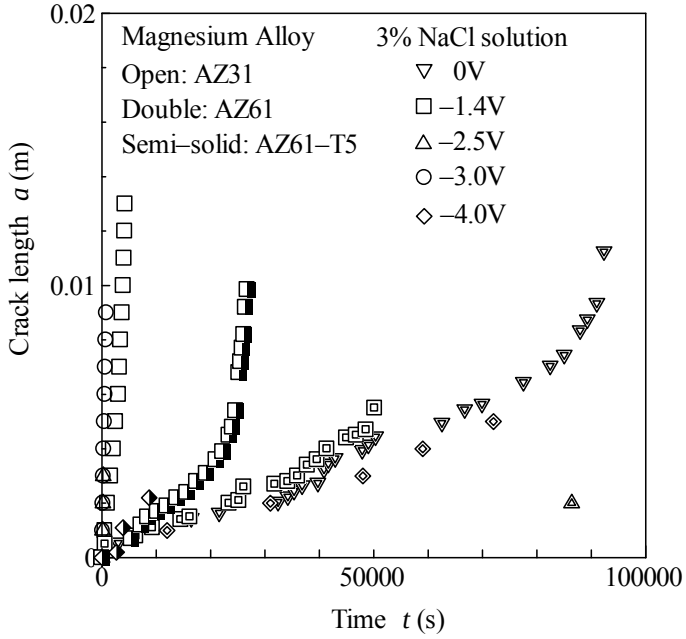

Figure 6. Relationship between crack length, a, and testing time, t

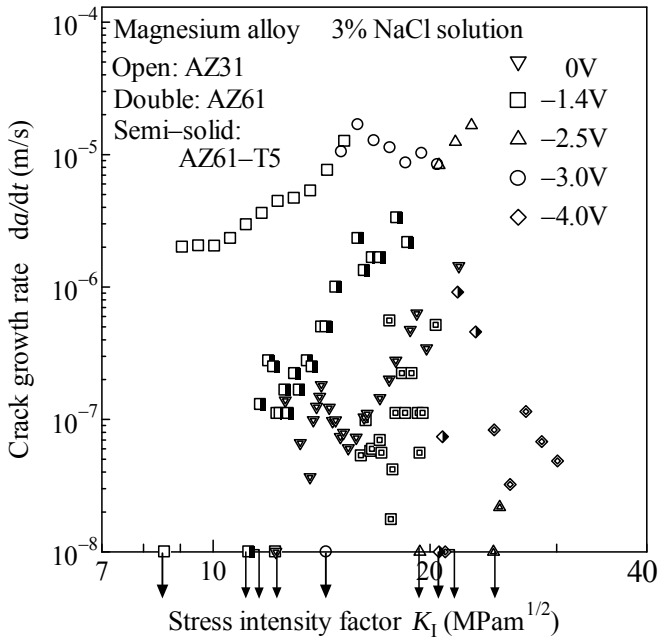

Figure 7. Relationship between crack growth rate, da/dt and stress intensity factor, K_I

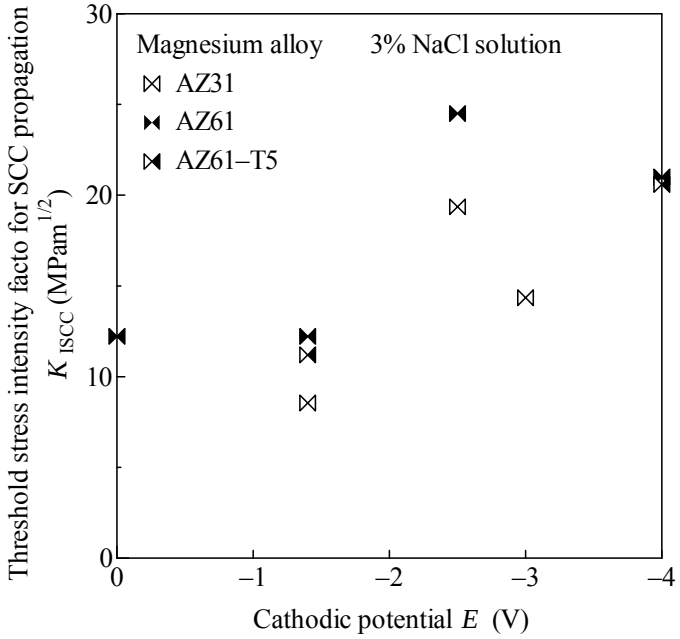

Figure 8. Relationship between threshold stress intensity factor for SCC propagation, K_{ISCC} and cathodic potential, E

3.2. Fracture surface observation

Fig. 9 shows the SEM micrographs showing the typical examples of fracture surfaces. As shown in Fig. 9 (a), the fracture surface of AZ31 under the cathodic potential of -1.4 V at K_I of 8.6 MPa m$^{1/2}$ was covered by corrosion products. However corrosion products became less on the fracture surface at K_I of 14 MPa m$^{1/2}$ as shown in Fig. 9 (b). Under the cathodic potentials of -2.5 V and -3.0 V, no corrosion products were observed as in Fig. 9 (c) and (d). In AZ61 and AZ61-T5, almost all of the fracture surfaces were covered by corrosion products and only a part of fracture surfaces were not covered as in Fig. 9 (e). As the cathodic potential became lower, corrosion products became less. Corrosion products on the fracture surfaces of AZ61 were less than those of AZ61-T5 comparatively. Some of the fracture surfaces of AZ61 remained their own morphologies under the cathodic potential of -4.0 V as in Fig. 9 (f). Except for the corrosion products, the fracture surface morphology is similar in all materials, i.e., fracture surfaces seem to be brittle covered with flat packets with fine steps without dimples as are observed in the fracture surfaces by fatigue tests [3].

4. Discussion

The crack growth rates of AZ31 specimens were much higher than those of AZ61 and AZ61-T5 specimens, which indicates the corrosion resistance of AZ31 is lower than those of AZ61 and AZ61-T5. Aluminum (Al) is added to AZ31 and AZ61 to enhance the strength and also to improve the corrosion resistance. So AZ61, which contains more Al than AZ31, exhibited better corrosion resistance. Comparing AZ61 and AZ61-T5, the crack growth rates of AZ61-T5 specimens were faster. It is attributed to the precipitated β phases which are more sensitive to corrosion than the matrix. But the β phases were precipitated along the limited region of grain boundaries so the corrosion resistance was not decreased as AZ31.

K_{ISCC} of AZ61 under the cathodic potential of -1.4 V is the same as that under the cathodic potential of 0 V, which indicates that the anodic dissolution occurred under the cathodic potential of -1.4 V as same as no cathodic potential is applied and the cathodic potential of -1.4 V did not act to decrease

the anodic dissolution. The same discussion could be made from the fracture surface observations, i.e., the fracture surface of AZ31 under the cathodic potential of -1.4 V at K_I of 8.6 MPa $m^{1/2}$ was covered with corrosion products. However, under the same cathodic potential of -1.4 V, corrosion products were less on the fracture surface at comparatively higher K_I of 14 MPa $m^{1/2}$. This is attributed to the difference of exposure time to the NaCl solution which is the corrosive environment. In the SCC tests conducted in the present study, the load was sustained once after a crack initiated to propagate. So K_I corresponds to the crack length. The fracture surface at low K_I was the area near the notch root and was exposed to the NaCl solution for longer time until a CT specimen was lead to final fracture than that at high K_I. So in the fracture surface at low K_I, the effect of the corrosive environment is large and the fracture surface became covered with corrosion products. The reason that almost all of the fracture surfaces of AZ61 and AZ61-T5, which are more insensitive to corrosion than AZ31, were covered with corrosion products is also explained by the exposure time to the corrosive environment. The crack growth rates of AZ61 and AZ61-T5 were slower and it took longer time until the final fractures than AZ31. Although AZ61 is insensitive to corrosion, the effect of longer exposure to the corrosive environment becomes large and so the fracture surfaces of AZ61 were also covered with corrosion products.

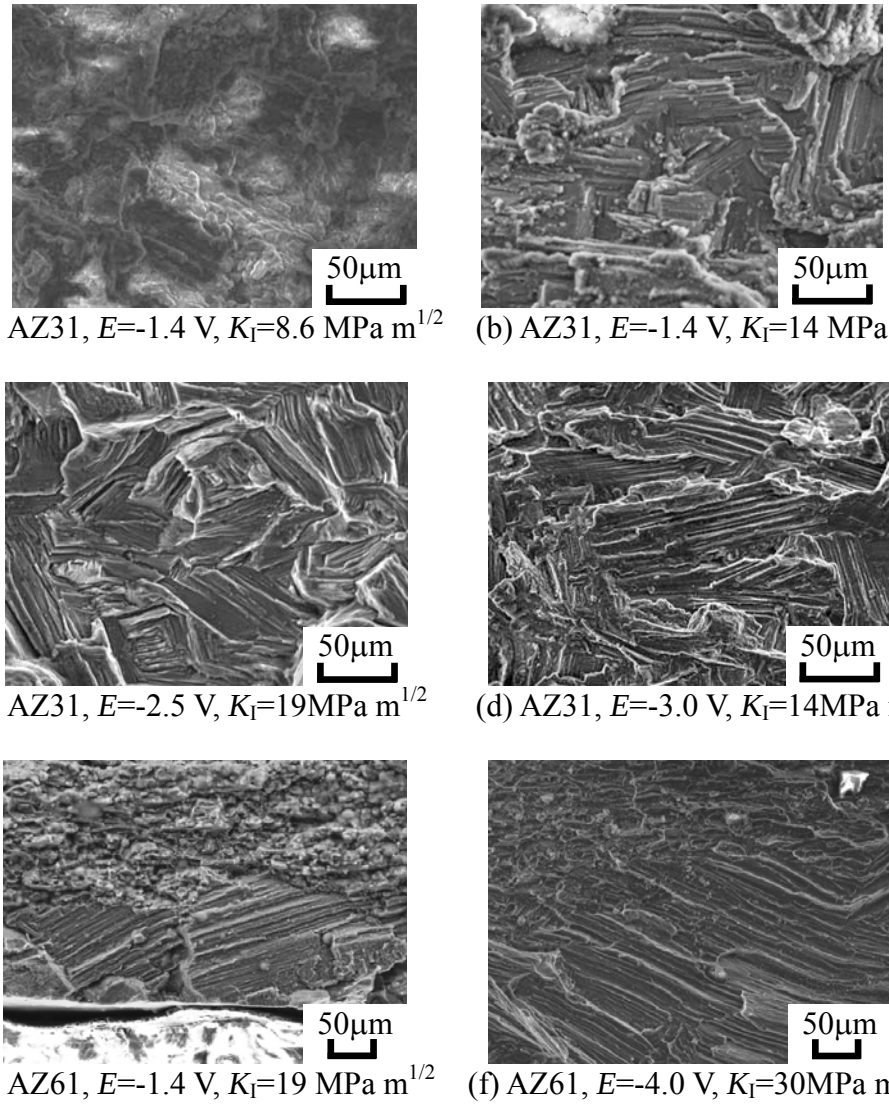

(a) AZ31, E=-1.4 V, K_I=8.6 MPa $m^{1/2}$ (b) AZ31, E=-1.4 V, K_I=14 MPa $m^{1/2}$

(c) AZ31, E=-2.5 V, K_I=19MPa $m^{1/2}$ (d) AZ31, E=-3.0 V, K_I=14MPa $m^{1/2}$

(e) AZ61, E=-1.4 V, K_I=19 MPa $m^{1/2}$ (f) AZ61, E=-4.0 V, K_I=30MPa $m^{1/2}$

Figure 9. SEM micrographs showing fracture surfaces

In AZ31 and AZ61, K_{ISCC} is the highest under the cathodic potential of -2.5 V in the boundary between the corrosion and immunity regions compared with those under higher and lower cathodic potentials. It is considered that under the higher cathodic potential, the corrosion is dominant and under the lower cathodic potential, the hydrogen embrittlement is dominant. The anodic dissolution is dependent on the cathodic potential, i.e., as the cathodic potential becomes lower, the anodic dissolution becomes decreased since the Mg phase becomes more stable than the Mg^{2+} phase as shown in Fig. 5 of the Pourbaix diagram, which is the reason that K_{ISCC} under the cathodic potential of -2.5 V is higher than that under the cathodic potential of -1.4 V. The generation of hydrogen molecules, H_2, should be also dependent on the cathodic potential, i.e., as the cathodic potential becomes lower, more H_2 are generated. Thus the lower cathodic potentials accelerated the hydrogen charging and K_{ISCC} becomes lower as the cathodic potential is lower than -2.5 V.

5. Conclusions

In the present study, the SCC tests were performed using the wrought magnesium alloys, AZ31, AZ61 and AZ61-T5 under the controlled cathodic potential and the effects of the anodic dissolution and the hydrogen embrittlement on the SCC behavior of Mg alloys were investigated. From the experimental results and the discussion, the following conclusions could be made:

(1) The crack growth rate of AZ31 was faster and K_{ISCC} of AZ31 was lower than those of AZ61 and AZ61-T5 under the same cathodic potential since the added Al acts to enhance the strength and to decrease the anodic dissolution.

(2) The crack growth rate of AZ61-T5 was faster and K_{ISCC} of AZ61-T5 was lower than those of AZ61 under the same cathodic potential since the precipitated β phases in AZ61-T5 are sensitive to hydrogen embrittlement.

(3) The crack growth rate depends on K_I. However in AZ31 the crack growth rate is not so sensitive to K_I. Especially the crack growth rate is insensitive to K_I under the cathodic potential of -3.0 V.

(4) In AZ31 and AZ61, K_{ISCC} under the cathodic potential of -2.5 V where the boundary between the corrosion and immunity regions is higher than K_{ISCC} under the higher cathodic potentials in the corrosion region where the anodic dissolution is dominant and K_{ISCC} under the lower cathodic potentials in the immunity region where the hydrogen embrittlement is dominant.

(5) In all materials, K_{ISCC} under the cathodic potential of -1.4 V was lower than that under the cathodic potentials of -3.0 V and -4.0 V.

(6) The amount of corrosion products depends on the cathodic potential and the exposure time to corrosive environment. Less corrosion products were observed on the fracture surfaces under the cathodic potentials of -3.0 V and -4.0 V than on the fracture surfaces under the cathodic potentials of 0 V and -1.4 V. A part of the fracture surfaces of AZ31 and almost all of the fracture surfaces of AZ61 and AZ61-T5 were covered with corrosion products where the exposure time was long.

References

[1] Y. Uematsu, T. Kakiuchi, M. Nakajima, Stress corrosion cracking of the wrouthg magnesium alloy AZ31 under controlled cathodic potentials, Materials Science and Engineering A, 531 (2012) 171–177.

[2] M. Pourbaix, Atlas of Electrochemical Equilibria in Aqueous Solutions, Pergamon Press, London, 1966.

[3] K. Tokaji, M. Nakajima, Y. Uematsu, Fatigue crack propagation and fracture mechanisms of wrought magnesium alloys in differenct environment, International Journal of Fatigue, 31 (2009) 1137–1143.